Plasmonic grating as a nonlinear converter-coupler

Nahid Talebi,[1,*] Mahmoud Shahabadi,[1] Worawut Khunsin,[2] and Ralf Vogelgesang[2]

[1]*Photonics Research Laboratory, Center of Excellence for Applied Electromagnetic Systems, School of Electrical and Computer Engineering, University of Tehran, North Kargar Ave., Tehran, Iran*
[2]*Max-Planck-Institut für Festkörperforschung, Heisenbergstrasse 1, 70569 Stuttgart, Germany*
[*]*n.talebi@ece.ut.ac.ir*

Abstract: The paper introduces a wavelength converter composed of a metallic finite 2-dimensional particle grating on top of an optical waveguide. The particles sustain plasmonic resonances which will result in the near-field enhancement and therefore, high conversion efficiency. Due to near-field interaction of the grating field with the propagating modes of the waveguide, the generated third harmonic wave is phase-matched to a propagating mode of the waveguide, while the fundamental frequency component is not coupled into the output waveguide of the structure. The performance of this structure is numerically investigated using a full-wave transmission line method for the linear analysis and a three-dimensional finite-difference time-domain method for the nonlinear analysis.

OCIS codes: (190.2620) Harmonic generation and mixing; (050.1950) Diffraction gratings; (240.6680) Surface plasmons; (230.7405) Wavelength conversion devices.

References and links

1. B. Lamprecht, A. Leitner, and F. R. Aussenegg, "SHG studies of plasmon dephasing in nanoparticles," Appl. Phys. B **68**(3), 419–423 (1999).
2. T. Zentgraf, A. Christ, J. Kuhl, and H. Giessen, "Tailoring the ultrafast dephasing of quasiparticles in metallic photonic crystals," Phys. Rev. Lett. **93**(24), 243901 (2004).
3. Z. J. Wu, X. K. Hu, Z. Y. Yu, W. Hu, F. Xu, and Y. Q. Lu, "Nonlinear plasmonic frequency conversion through quasiphase matching," Phys. Rev. B **82**(15), 155107 (2010).
4. M. D. Wissert, K. S. Ilin, M. Siegel, U. Lemmer, and H. J. Eisler, "Coupled nanoantenna plasmon resonance spectra from two-photon laser excitation," Nano Lett. **10**(10), 4161–4165 (2010).
5. T. Uthayakumar, C. P. Jisha, K. Porsezian, and V. C. Kuriakose, "Switching dynamics of a two- dimensional nonlinear directional coupler in a photopolymer," J. Opt. **12**(1), 015204 (2010).
6. S. Kim, J. H. Jin, Y. J. Kim, I. Y. Park, Y. Kim, and S. W. Kim, "High-harmonic generation by resonant plasmon field enhancement," Nature **453**(7196), 757–760 (2008).
7. K. Dolgaleva and R. W. Boyd, "Laser gain media based on nanocomposite materials," J. Opt. Soc. Am. B **24**(10), A19–A25 (2007).
8. R. S. Bennink, Y. K. Yoon, R. W. Boyd, and J. E. Sipe, "Accessing the optical nonlinearity of metals with metal-dielectric photonic bandgap structures," Opt. Lett. **24**(20), 1416–1418 (1999).
9. D. Rosenblatt, A. Sharon, and A. A. Friesem, "Resonant grating waveguide structures," IEEE J. Quantum Electron. **33**(11), 2038–2059 (1997).
10. R. Magnusson and S. S. Wang, "New principle for optical filters," Appl. Phys. Lett. **61**(9), 1022–1024 (1992).
11. D. L. Brundrett, E. N. Glytsis, and T. K. Gaylord, "Normal-incidence guided-mode resonant grating filters: design and experimental demonstration," Opt. Lett. **23**(9), 700–702 (1998).
12. S. Peng and G. M. Morris, "Resonant scattering from two-dimensional gratings," J. Opt. Soc. Am. A **13**(5), 993–1005 (1996).
13. R. W. Day, S. S. Wang, and R. Magnusson, "Filter-response line shapes of resonant waveguide gratings," J. Lightwave Technol. **14**(8), 1815–1824 (1996).
14. D. K. Jacob, S. C. Dunn, and M. G. Moharam, "Design considerations for narrow-band dielectric resonant grating reflection filters of finite length," J. Opt. Soc. Am. A **17**(7), 1241–1249 (2000).
15. A. Selle, C. Kappel, M. A. Bader, G. Marowsky, K. Winkler, and U. Alexiev, "Picosecond-pulse-induced two-photon fluorescence enhancement in biological material by application of grating waveguide structures," Opt. Lett. **30**(13), 1683–1685 (2005).
16. S. Soria, T. Katchalski, E. Teitelbaum, A. A. Friesem, and G. Marowsky, "Enhanced two-photon fluorescence excitation by resonant grating waveguide structures," Opt. Lett. **29**(17), 1989–1991 (2004).

#156396 - $15.00 USD Received 12 Oct 2011; revised 9 Dec 2011; accepted 9 Dec 2011; published 9 Jan 2012

17. C. Kappel, A. Selle, M. A. Bader, and G. Marowsky, "Resonant double-grating waveguide structures as inverted Fabry-Perot interferometers," J. Opt. Soc. Am. B **21**(6), 1127–1136 (2004).
18. A. M. Ferrie, Q. Wu, and Y. Fang, "Resonant waveguide grating imager for live cell sensing," Appl. Phys. Lett. **97**(22), 223704 (2010).
19. H. N. Daghestani and B. W. Day, "Theory and applications of surface plasmon resonance, resonant mirror, resonant waveguide grating, and dual polarization interferometry biosensors," Sensors (Basel Switzerland) **10**(11), 9630–9646 (2010).
20. J. Y. Andersson, L. Lundqvist, and Z. F. Paska, "Quantum efficiency enhancement of AlGaAs/GaAs quantum-Well Infrared detectors using a wave-guide with a grating coupler," Appl. Phys. Lett. **58**(20), 2264–2266 (1991).
21. S. Peng and G. M. Morris, "Resonant scattering from two-dimensional gratings," J. Opt. Soc. Am. A **13**(5), 993–1005 (1996).
22. N. Talebi and M. Shahabadi, "All-optical wavelength converter based on a heterogeneously integrated GaP on a silicon-on-insulator waveguide," J. Opt. Soc. Am. B **27**(11), 2273–2278 (2010).
23. T. Zentgraf, S. Zhang, R. F. Oulton, and X. Zhang, "Ultranarrow coupling-induced transparency bands in hybrid plasmonic systems," Phys. Rev. B **80**(19), 195415 (2009).
24. T. Utikal, T. Zentgraf, T. Paul, C. Rockstuhl, F. Lederer, M. Lippitz, and H. Giessen, "Towards the origin of the nonlinear response in hybrid plasmonic systems," Phys. Rev. Lett. **106**(13), 133901 (2011).
25. Y. Dumeige, F. Raineri, A. Levenson, and X. Letartre, "Second-harmonic generation in one-dimensional photonic edge waveguides," Phys. Rev. E Stat. Nonlin. Soft Matter Phys. **68**(6), 066617 (2003).
26. B. Maes, P. Bienstman, and R. Baets, "Modeling second-harmonic generation by use of mode expansion," J. Opt. Soc. Am. B **22**(7), 1378–1383 (2005).
27. B. Maes, P. Bienstman, R. Baets, B. B. Hu, P. Sewell, and T. Benson, "Modeling comparison of second-harmonic generation in high-index-contrast devices," Opt. Quantum Electron. **40**(1), 13–22 (2008).
28. C. M. Reinke, A. Jafarpour, B. Momeni, M. Soltani, S. Khorasani, A. Adibi, Y. Xu, and R. K. Lee, "Nonlinear finite-difference time-domain method for the simulation of anisotropic, $\chi^{(2)}$ $\chi^{(3)}$ " J. Lightwave Technol. **24**(1), 624–634 (2006).
29. R. M. Joseph and A. Taflove, "FDTD Maxwell's equations models for nonlinear electrodynamics and optics," IEEE Trans. Antenn. Propag. **45**(3), 364–374 (1997).
30. J. Dorfmüller, R. Vogelgesang, R. T. Weitz, C. Rockstuhl, C. Etrich, T. Pertsch, F. Lederer, and K. Kern, "Fabry-Pérot resonances in one-dimensional plasmonic nanostructures," Nano Lett. **9**(6), 2372–2377 (2009).
31. T. Verbiest, K. Clays, and V. Rodriguez, *Second-Order Nonlinear Optical Characterization Technique* (CRC Press, 2009) 96–97.
32. P. G. Etchegoin, E. C. Le Ru, and M. Meyer, "An analytic model for the optical properties of gold," J. Chem. Phys. **125**(16), 164705 (2006).
33. J. B. Schneider, "Understanding the finite-difference time-domain method" (2010), retrieved December 5th, 2011, www.eecs.wsu.edu/~schneidj/ufdtd.
34. M. Shahabadi, S. Atakaramians, and N. Hojjat, "Transmission line formulation for the full-wave analysis of two-dimensional dielectric photonic crystals," IEEE P Sci.Meas. Tech. **151**(5), 327–334 (2004).
35. P. B. Johnson and R. W. Christy, "Optical-constants of noble-metals," Phys. Rev. B **6**(12), 4370–4379 (1972).
36. L. Gu, W. Sigle, C. T. Koch, B. Ogut, P. A. van Aken, N. Talebi, R. Vogelgesang, J. Mu, X. Wen, and J. Mao, "Resonant wedge-plasmon modes in single-crystalline gold nanoplatelets," Phys. Rev. B **83**(19), 195433 (2011).
37. R. W. Boyd, *Nonlinear Optics* (Academic Press, 2008).
38. F. Hache, D. Ricard, and C. Flytzanis, "Optical nonlinearities of small metal particles - surface-mediated resonance and quantum size effects," J. Opt. Soc. Am. B **3**(12), 1647–1655 (1986).

1. Introduction

Exploiting optical nonlinearity of metals has been a vigorous area of research and development in the last decades. In comparison with dielectrics, metals have intrinsically higher odd-order nonlinear susceptibility. This makes them suitable in realizations of optical up-converters with a variety of applications, such as tailoring the dynamics of plasmonic modes [1, 2], wavelength conversion using quasi-phase matched plasmonic photonic crystals [3], nonlinear optical excitation for dark field microscopy [4], and all-optical switching [5]. Moreover, enhancement of the optical near-field with localized plasmonic resonances of metallic nano-particles greatly increases the conversion efficiency of the nonlinear process. This effect has been utilized to achieve higher harmonic generation from a host medium using plasmonic resonances of bow-tie antennas [6]. More fundamental research has been carried out to utilize localized plasmonic resonances in metal-dielectric composite materials in the form of either Maxwell-Garnet [7] or layered photonic band gap structures [8].

Resonant grating waveguide structures which are composed of single or double diffraction gratings on top of a high refractive index slab waveguide have been extensively investigated

#156396 - $15.00 USD Received 12 Oct 2011; revised 9 Dec 2011; accepted 9 Dec 2011; published 9 Jan 2012

in the literature [9–12]. The grating integrated on top of the waveguide enables the coupling of radiated beams into the propagating modes of waveguide by mapping the wave vector of waveguide modes into the light cone. Such structures have been exploited in extremely narrow line reflection filters [13, 14], enhancement of two-photon fluorescence excitation [15, 16], inverted Fabry-Pérot interferometers [17], optical biosensors [18, 19], and enhancement of quantum efficiency of quantum-well infrared detectors [20].

Considering time reversal, in the presence of the grating the guided modes can also excite radiation modes of the structure. Resonances in the reflection and transmission of such structures can be attributed to the interference of radiation due to diffraction of the guided modes and the directly reflected and transmitted radiation. It is noteworthy that most resonant grating waveguide structures studied so far are periodic in one dimension only, with translational invariance in the second direction. Only a few attempts have been made to investigate the coupling to photonic waveguides with gratings having 2-dimensional periodicity [21], as studied here.

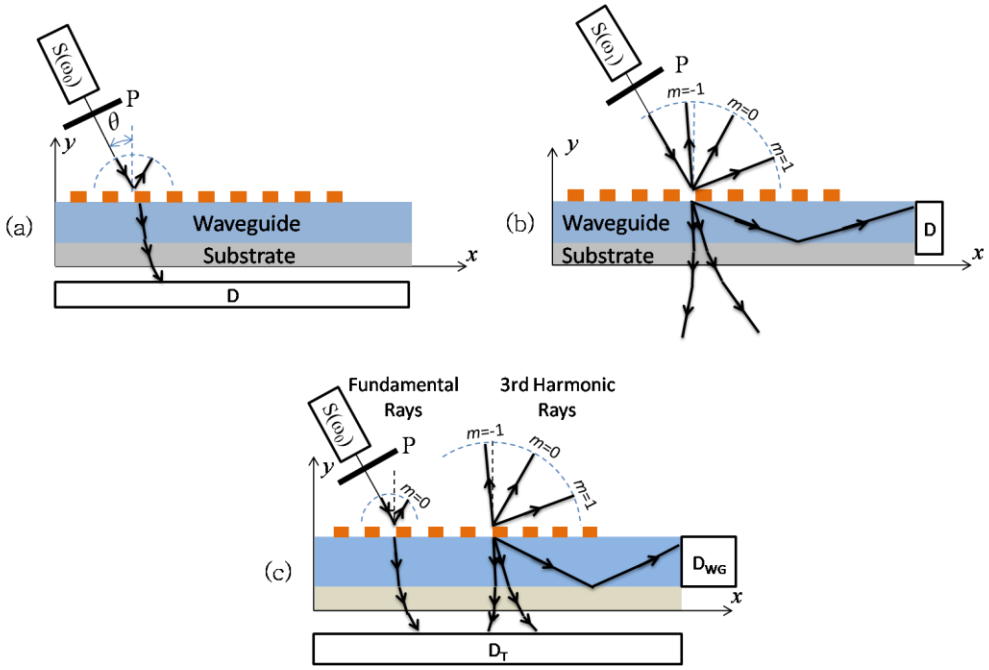

Fig. 1. Realization of a wavelength converter coupler with nonlinear grating. (a) A linear grating on the top surface of a slab waveguide. Here, the frequency ω_0 is not coupled to the slab waveguide. (b) The same grating acts as a coupler at a frequency of $\omega_1 > \omega_0$. The grating exhibits anomalies at a diffraction order, by mapping the phase-constant of the slab waveguide into the light cone. (c) A nonlinear grating which can be used as a coupler at the third-harmonic frequency without any anomaly at the fundamental frequency. D stands for Detector, P for polarizer, and S for Source.

We report on an optical wavelength converter, whose critical element is a plasmonic nonlinear grating coupler on the top surface of a slab waveguide. The nonlinear grating is comprised of gold nano-rod antennas. Their geometry is tuned such that their plasmonic resonance is at the fundamental frequency. Due to (nearly perfect) inversion symmetry of the gold nano-particles, the bulk second-harmonic generation is essentially forbidden. We therefore consider only the third-order nonlinear susceptibility of gold nano-particles. The period of the grating has been designed on the one hand to match the wave vector of the generated third-harmonic radiation to the phase-constant of the waveguide mode. The

#156396 - $15.00 USD Received 12 Oct 2011; revised 9 Dec 2011; accepted 9 Dec 2011; published 9 Jan 2012

fundamental beam, on the other hand, is not coupled to the waveguide, i.e., it is reflected and transmitted only into the zeroth diffraction order as shown in Fig. 1. Thus, there is no need to filter out the fundamental beam at the output of D_{WG} (Output detector), while both the fundamental and converted beams are present at the location of D_T. This detector is placed just below the substrate, enabling the detection of near-field intensities of the electromagnetic field. In [22] we had introduced a nonlinear dielectric grating, which couples second harmonic radiation into an underlying silicon-on-insulator waveguide. The nonlinear metallic grating introduced here uses plasmonic particle resonances for enhanced up-conversion of radiation. This is exclusively coupled into propagating modes of the underlying waveguide via the independently designed grating arrangement of the particles; the fundamental radiation is not coupled to the waveguide.

Since, at first glance, our structure design might seem similar to hybrid grating-waveguide approaches such as used in [23, 24], we briefly discuss the crucial distinctions. Whereas the latter uses 1-dimensional gratings, illuminated with p-polarization, we investigate 2-dimensional gratings, excited in s-polarization. In hybrid grating-waveguides two resonant systems are coupled at the fundamental frequency – often in a Fano-type fashion [23, 24] – to form new hybrid modes. In our design only the finite 3-dimensional metallic nano-rod antennas are individually resonant and may be thought of as the sole third harmonic generator. This third harmonic radiation is subsequently coupled into propagating modes of the waveguide, where they are sustained even at great distances from the converter-coupler area. Moreover, exploiting the 3-dimensional resonating system with nano-rods will result in a huge field-enhancement factor, about 2 orders of magnitude higher than the field enhancement achievable with 2-dimensional gratings. In toto, whereas the generation of third harmonic radiation, its coupling to, and propagation in the waveguide are intricately fused in hybrid structures, they appear conceptually and structurally separated in the device we propose here.

The numerical methods exploited so far to simulate nonlinear photonic structures fall into two broad categories: analytical modeling such as coupled mode theory [25], and numerical methods such as eigen-mode expansions [26], the time-domain beam-propagation method (TD-BPM) [27], the finite-difference frequency-domain (FDFD) and the finite-difference time-domain method (FDTD). Analytical modeling is not appropriate for structures of complex geometries. Eigen-mode expansion methods assume the slowly varying envelope approximation. A time differencing procedure is utilized to solve the two resulting coupled equations for the fundamental and the second-harmonic waves. TD-BPMs work with paraxial wave propagation. The frequency-domain methods like FDFD may also be used following the undepleted pump approximation. Among these methods, however, FDTD appears most versatile and suitable in modeling various nonlinear processes such as wave mixing and harmonic generation [22, 28, 29]. This method is used here to investigate the nonlinear performance of the structure.

#156396 - $15.00 USD Received 12 Oct 2011; revised 9 Dec 2011; accepted 9 Dec 2011; published 9 Jan 2012

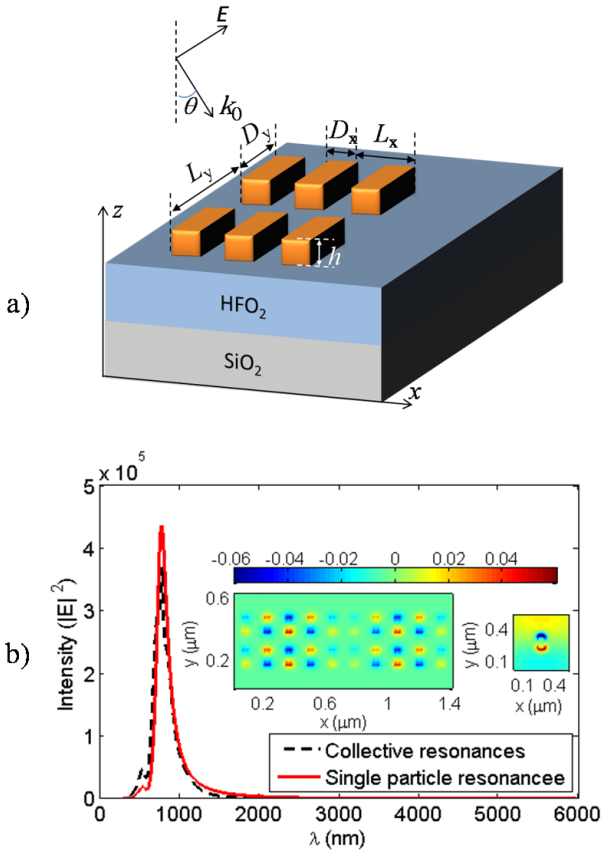

Fig. 2. (a) The configuration of the proposed wavelength converter, which is composed of a 2-dimentional grating of Au nano-rod antennas on top of a HfO_2 slab waveguide. (b) Single particle and collective resonances of the near-field intensity for Au nano-particles of Fig. 2(a), with the parameters $D_x = 40nm$, $D_y = 120nm$, $h = 40nm$, $L_x = 140nm$, and $L_y = 240nm$. The insets show the field profile for the z-component of the electric field at a specific time over the structures at a distance of only 10 nm, for both a single particle and a finite array of nano-particles.

2. Structure and linear analysis

Figure 2(a) shows the structure of the proposed wavelength converter. This multi-layer structure is comprised of a finite array of gold nano-particles on a slab waveguide. Due to the in-plane inversion symmetry of the gold nano-particles used here, generation of second harmonic signal is only limited to the interface at which the inversion symmetry is broken, therefore, the effective second-order nonlinear susceptibility is of smaller magnitude than the third-order nonlinear susceptibility of gold. The grating is exposed to a beam at the fundamental frequency ω_0. The generated third harmonic signal (THS) is radiated into several diffraction orders, whereas for the fundamental frequency only the zeroth-order is available through a careful design of grating periodicity, i.e., $L_x << \lambda_0$ and $L_y << \lambda_0$. In order to couple the THS to the propagating modes of the waveguide, the following phase matching condition must be satisfied:

$$k_x(3\omega_0) + \frac{2m\pi}{L_x} = \beta(3\omega_0) \qquad (1)$$

#156396 - $15.00 USD Received 12 Oct 2011; revised 9 Dec 2011; accepted 9 Dec 2011; published 9 Jan 2012

Here, $k_x(3\omega_0) = 3k_0(\omega)\sin(\theta)$ is the wave-vector of the THS projected on the x-axis, L_x is the periodicity of the structure in the x-direction, $m = ..., -1, 0, 1, ...$ denotes different diffraction orders, and $\beta(3\omega_0)$ is the propagation constant of the TE_y or TM_y modes of the waveguide at the third harmonic frequency. We assume that the fundamental beam is at a wavelength of $\lambda_0 = 800nm$, and that the HfO_2 layer used here has a thickness of 180nm. The analytical relation for the dispersion diagram of the bare slab waveguide (far away from the converter-coupler area) shows the values of $\beta_{TM_y}(3\omega_0) = 4.797\times10^7\ 1/m$ and $\beta_{TE_y}(3\omega_0) = 4.218\times10^7\ 1/m$ for the TM_y and TE_y modes of the waveguide, respectively. The fundamental wavelength is λ_0 = 800nm, and the height of the HfO_2 slab waveguide is 180nm. Using Eq. (1), and considering $L_x = 140nm$, which is small enough in comparison with the fundamental wavelength, one can approximately compute the angles at which the phase-matching conditions are satisfied. These are $\theta = 7.54^\circ$ and $\theta = -6.58^\circ$, for the TM_y and TE_y modes of the waveguide, respectively. The negative angle means that the second-order mode is in the opposite direction of propagation compared with the incident beam. This is because of the influence of the periodic grating which folds the band-diagram of the structures at the boundary of the Brillouin zone (X-point).

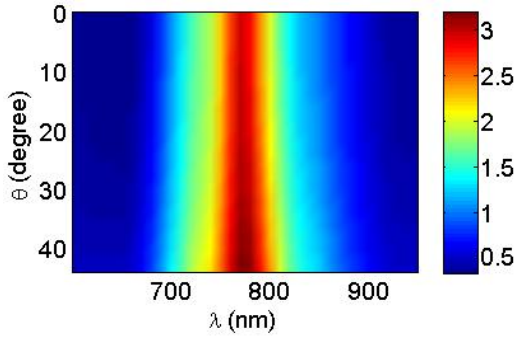

Fig. 3. Extinction spectrum versus the angle of incidence (θ) and free-space wavelength (λ) for $0 \le \theta \le 45$ and $600nm \le \lambda \le 950nm$, computed for the structure depicted in Fig. 2(a) illuminated with an s-polarized plane-wave. The color bar is in arbitrary linear units

The Au nanoparticles used here as the elements of the nonlinear grating show plasmonic resonances at the fundamental wavelength of 800nm. Because of the quasi-1-dimensional Fabry-Pérot-like plasmonic resonance inside the nano-rods [30], a huge field enhancement is obtained with a considerable impact on the generated intensity of the THS. This can be described with Eq. (2),

$$I^{THS}(3\omega_0) \propto \left|\chi^{(1)}(3\omega_0)L(3\omega_0)\left(\chi^{(1)}(\omega_0)L(\omega_0)\right)^3\right|^2 \left(I^i(\omega_0)\right)^3 \qquad (2)$$

Here, $I^{THS}(3\omega_0)$ is the generated third-harmonic intensity, $L(\omega)$ is the local electric-field enhancement factor [31], $\chi^{(1)}(\omega)$ is the dispersive linear susceptibility of gold, and $I^i(\omega_0)$ is the intensity of the incident beam at the fundamental frequency. Figure 2(b) shows the computed near-field intensity spectrum for a single gold rectangular nanoparticle with the parameters $D_x = 40nm$, $D_y = 120nm$, and $h = 40nm$ defined in Fig. 2(a), and also for an array of the same nanoparticles with a periodicity of $L_x = 140nm$ and $L_y = 240nm$ along the

#156396 - $15.00 USD Received 12 Oct 2011; revised 9 Dec 2011; accepted 9 Dec 2011; published 9 Jan 2012

x and y directions, respectively. A 3D-FDTD method has been used for these calculations with a Drude model extended by two critical point functions for the fitting of the gold permittivity, as reported in [32]. Second-order absorbing boundary conditions have been used to terminate the solution domain. The solution domain is discretized with unit-cells of the size of $10nm \times 10nm$. The magnitude of the electric field is computed right above the rectangular nanoparticles at a distance of 10nm. For calculating the spectrum, a wide-band y-polarized excitation in the form of a Ricker-wavelet is introduced as an additive source [33], while for the spatial distribution a Gaussian function has been used. A discrete Fourier transform of the time-domain electric field components allows computing the frequency spectrum. Evidently the collective response of the whole array shows the same resonant behavior as a single particle, thanks to the large spacing between the individual elements.

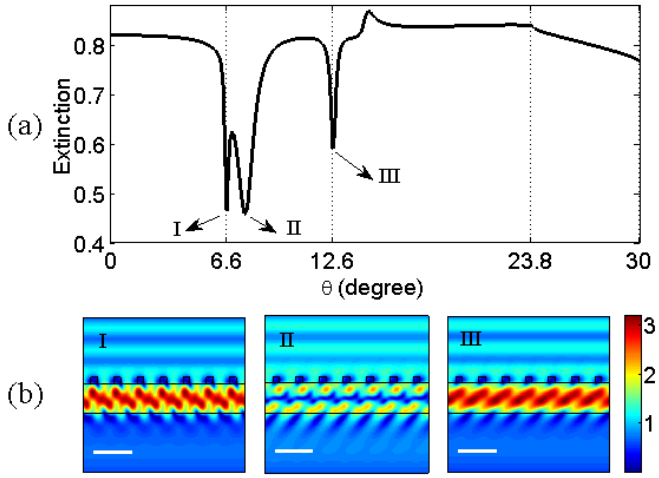

Fig. 4. (a) Extinction spectrum versus θ at $\lambda = 267nm$, computed for the proposed structure of Fig. 2(a), illuminated with an s-polarized plane-wave. (b) Magnitude of the y-component of the electric field ($|E_y|$) for the anomalies of the extinction spectrum at $\lambda = 267\text{nm}$ and for illuminating the structure with a y-polarized plane wave at angles of anomaly. The scale bars are all 150nm. The color bar is in arbitrary linear units

In order to investigate the far-field response of the grating, the full-wave transmission line (TL) method [34] has been used to calculate the extinction spectrum ($-\ln(T)$) of an infinite periodic structure with the same particles as above. Figure 3 shows the calculated extinction spectrum versus the angle of incidence for the wavelengths $\lambda = 600nm \sim 950nm$. Clearly, the response to s-polarized excitation of a grating of gold nanoparticles is largely independent of the angle of incidence over the intervals $0 \le \theta \le 45$ degrees and $600nm \le \lambda \le 950nm$. The absence of any strong grating response is due the period of the grating along the x-axis being much smaller than the wavelength of the incident wave, which leaves the plasmonic resonances uncoupled from the propagating modes of the slab waveguide. In other words, this structure does not support a waveguide-polariton quasi-particle like the one introduced in [2, 23, 24]. This fact is advantageous in the present case, since its enhancement factor is rather constant over a wide range of incident angles of the input beam. Figure 4 shows the extinction spectrum versus θ at $\lambda = 267nm$, i.e., at the wavelength of the generated THS. Three sharp anomalies are visible in the extinction spectrum. The anomalies at $\theta = 6.6^\circ$ and $\theta = 7.7^\circ$ arein agreement with the results estimated above using Eq. (1). The anomaly at $\theta = 12.6^\circ$ can also be obtained using Eq. (1) with the propagation constant of the lower order TM_y mode.

#156396 - $15.00 USD Received 12 Oct 2011; revised 9 Dec 2011; accepted 9 Dec 2011; published 9 Jan 2012

Figure 4(b) shows the magnitude of the E_y field component at $\lambda = 267$nm when the structure is exposed to a y-polarized plane wave at $\theta = 6.6°$, $\theta = 7.7°$, and $\theta = 12.6°$, respectively. A sharp Fano resonance is visible at $\theta = 6.6°$ which is mainly due to the coupling of the two individual resonances at $\theta = 6.6°$ and $\theta = 7.7°$.

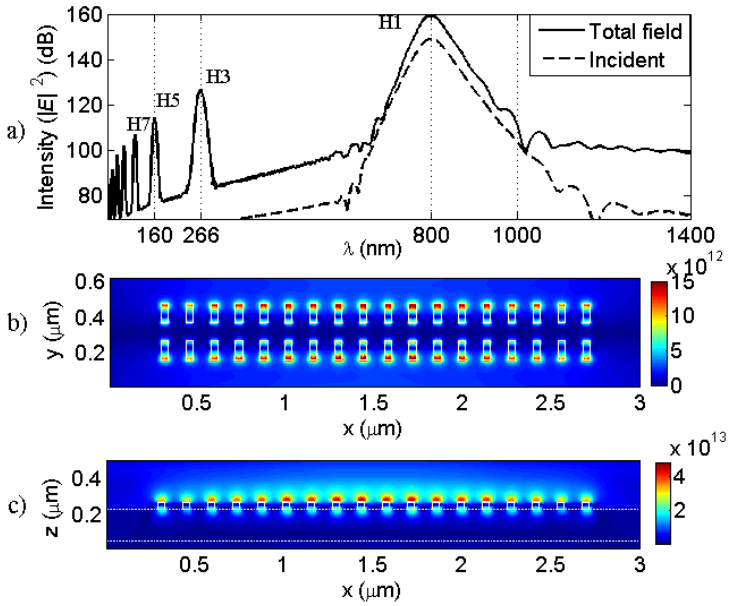

Fig. 5. (a) Average intensity of the electric field over the grating of the nanoparticles versus the free-space wavelength, computed for the total field and the incident field. The incident optical pulse corresponds to a typical output beam of a pulsed Ti:Sapphire laser, which impinges the sample at normal incidence. Magnitude of $E_z(\vec{r},\omega_0)$ at the fundamental wavelength for (b) the xy-plane at 10nm above the structure, and (c) the xz-plane formed by cutting the first row of the nano-particles at 10nm from the front side. The color bars are in arbitrary linear units.

3. Nonlinear analysis using FDTD method

In order to investigate the performance of the converter-coupler introduced in this paper, we apply a nonlinear, 3-dimensional FDTD method previously developed in our lab [22]. The simulation domain is discretized with uniform unit-cells of size 10 nm. We neglect second-order terms as discussed above. The relation between the polarization vector and the electric field is assumed to be:

$$P_\alpha(r,t) = P_\alpha^{(L)}(r,t) + \varepsilon_0 \sum_{\beta\gamma\tau} \chi^{(3)}_{\alpha\beta\gamma\tau}(r) E_\beta(r,t) E_\gamma(r,t) E_\tau(r,t) \qquad (3)$$

Here, the first term denotes the linear polarization vector, whereas the second represents the nonlinear polarization. $\left\{\chi^{(3)}_{\alpha\beta\gamma\tau}\right\}$ with $\{\alpha,\beta,\gamma,\tau\} \in \{x,y,z\}$ are the elements of the third-order nonlinear susceptibility tensor. The linear dispersive permittivity of the gold nanoparticles is modeled by fitting a Drude model extended by two critical point functions [32] to the experimental data reported in [35]. The same model has also been used in [36] by the authors, where very good agreement was found between the numerical results and experimental values obtained from electron-energy-loss spectroscopy of single-crystalline gold nanoplatelets. For isotropic media like Au, a simplified form of Eq. (3) can be used to drive the constitutive relation for the D-field as:

#156396 - $15.00 USD Received 12 Oct 2011; revised 9 Dec 2011; accepted 9 Dec 2011; published 9 Jan 2012

$$D = P^{(L)} + \varepsilon_0 \begin{bmatrix} \varepsilon_\infty + \chi^{(3)}|\mathrm{E}|^2 & 0 & 0 \\ 0 & \varepsilon_\infty + \chi^{(3)}|\mathrm{E}|^2 & 0 \\ 0 & 0 & \varepsilon_\infty + \chi^{(3)}|\mathrm{E}|^2 \end{bmatrix} \begin{bmatrix} E_x \\ E_y \\ E_z \end{bmatrix} \qquad (4)$$

for which we have considered only the simple AC-Kerr effect [37]. The value of the nonlinear susceptibility used here is $\chi^{(3)} = 1\times10^{-20}\, m^2/V^2$ for gold nanoparticles [38] and $\chi^{(3)} = 0$ for the surrounding medium. It should be noted that the nonlinear behavior of HfO_2 and quartz is neglected in comparison to that of gold. The magnetic field and the electric displacement vector (D) are updated in every iteration. For updating the electric field, a Newton iteration procedure is utilized to compute the electric field from the previously updated electric displacement using Eq. (4) [29].

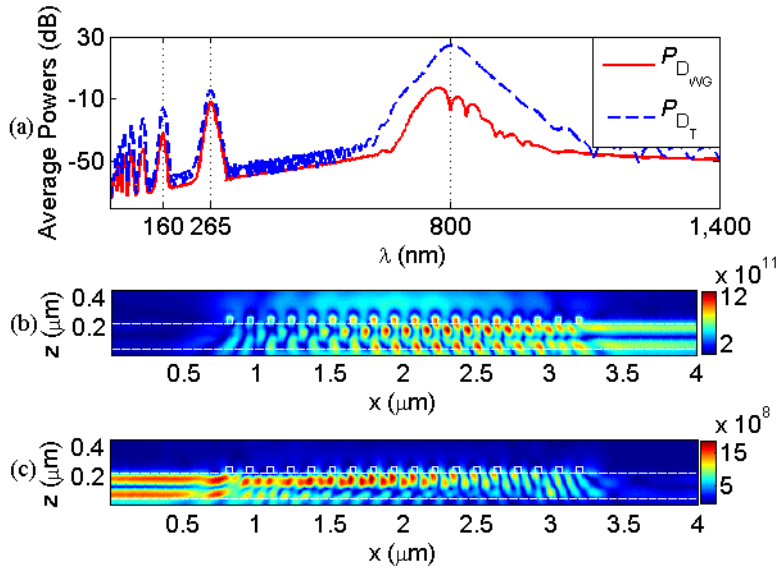

Fig. 6. (a) The power spectrum of the detected signals computed using Eq. (5), for illuminating the structure at the fundamental wavelength ($\lambda = 800nm$) and at an angle of $\theta = 7^\circ$ from normal to the grating. For the excitation an s-polarized spatial- Gaussian optical pulse with a broadening of 1.5λ and the temporal duration of 50 fs has been used. The spatial distribution of the generated (b) $E_y(\vec{r}, 3\omega_0)$ (c) $H_y(\vec{r}, 3\omega_0)$ at $\lambda = 267nm$. The color bars are in arbitrary linear units.

The simulation domain contains a total number of 36 nanoparticles on the HfO_2 waveguide with a quartz substrate. The particles are arranged in two rows along the y-axis with $D_x = 40nm$, $D_y = 120nm$, $L_x = 140nm$, and $L_y = 240nm$. In order to excite the plasmonic resonances of the gold nanoparticles, the structure is excited with a TM_y optical pulse of 50 fs duration and a carrier wavelength of 800nm.

As the spatial distribution of the optical pulse a Gaussian function with $W = 1.5\lambda$ is used in which W is the beam-width of the optical pulse at the half-maximum intensity. The peak power of the excitation introduced here is P_{max} = 61kW, which is smaller than the one reported in [6], which is 100kW. The maximum intensity of the excitation (or magnitude of the Poynting vector) is $I_{max} \approx 1.8\times10^{13}\, W\, cm^{-2}$. Figure 5(a) shows the average intensity of the electric field computed at test points located 10nm above the nanoparticles for the total and

#156396 - $15.00 USD Received 12 Oct 2011; revised 9 Dec 2011; accepted 9 Dec 2011; published 9 Jan 2012

incident fields at normal incidence. Generation of higher harmonics up to an order of 11 is observed in this figure. The local field enhancement factor at the fundamental wavelength is approximately 60 dB just outside the top surface of the array structure. Nevertheless, the produced THS is not particularly strong, which is mainly due to the dissipative nature of gold at the third harmonic: $\chi^{(L)}(3\omega_0) = -0.5574 + 9.7525i$. That is, the produced THS is strongly absorbed inside the nanoparticles. This can also be computed from the diffraction efficiency spectrum. Normalized dissipated power is computed from $P_d = 1 - \sum_{i,j} r_{ij} - \sum_{i,j} t_{ij}$ in which r_{ij} and t_{ij} are the reflection and transmission coefficients. Such calculations show that the dissipated power is about 38% at $\lambda = 267nm$.

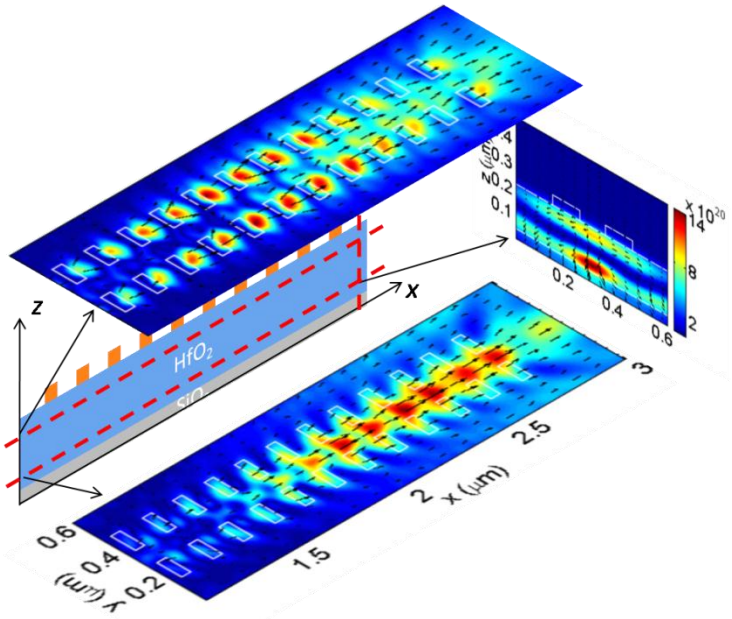

Fig. 7. Magnitude of the x-component of the Poynting vector $S_x(\vec{r},\omega)$ at $\lambda = 267nm$ computed for different cross-sections of the structure. For the excitation, an s-polarized Gaussian optical pulse with the broadening of 1200nm and temporal duration of 50 fs at the central wavelength of 800nm has been used. The color bars are in arbitrary linear units.

Figure 5(b) and (c) show the spatial distribution for the magnitude of the Fourier-transform of the z-component of the electric field at the fundamental wavelength. Figure 5(b) depicts these values in the xy-plane 10nm above the structure, and Fig. 5(c) gives these values in the xz-plane passing through the first row of the nanoparticles 10nm away from the front side. From Fig. 5(c) we conclude that the maximum enhancement factor occurs just above the nanoparticles, and inside the nanoparticles the field penetrates with a skin-depth of about 10 nm. Figure 6(a) shows the average power computed at the position of the detectors depicted in Fig. 1. These power spectra are calculated as Fourier-transforms of the E and H fields, as:

$$P_{g,t}(\omega) = \tfrac{1}{2}\mathrm{Re}\left(\int_{S_{WG},\,S_T} E(\omega) \times H^*(\omega) \cdot dS_{g,t} \right) \qquad (5)$$

in which S_{WG} and S_t are the cross-sections of the detectors. Figure 6(b) and 6(c) show the magnitude of the Fourier-transform of the y-component of the electric field and the y-

#156396 - $15.00 USD Received 12 Oct 2011; revised 9 Dec 2011; accepted 9 Dec 2011; published 9 Jan 2012

component of the magnetic field at third harmonic frequency. The guided third harmonic power is divided into the TM_y and TE_y modes of the waveguide. Due to the angular extent of the Gaussian excitation beam used here, TM_y and TE_y modes are excited simultaneously (see also Fig. 4). Curiously, though, they propagate away from the coupling region in opposite directions, as can be clearly seen from Fig. 6(b) and Fig. 6(c). A sharp dip is observed in the logarithmic power spectrum $P_{D_{WG}}$ at $\lambda = 800nm$, which verifies the phase matching condition described by Eq. (1). The suppression is not perfect, though, presumably due to direct illumination of the detector in the waveguide by tails of the Gaussian excitation, which are refracted at the air/waveguide interface and diffracted at the finite grating. Thus a finite portion of the field strength of the fundamental frequency component is present at this location inside the waveguide. However, as these rays cannot excite the propagating fundamental frequency modes, these field components die off exponentially along x in the waveguide. In an experimental study of such a converter coupler structure, the spectrum would be picked up at much greater distances than the detector simulated here. We expect a much improved suppression of the fundamental signal under these circumstances. The number of unit-cells used here along the x-direction is only 18. Obviously, a sharper and deeper resonance may be achieved if the number of the grating elements increases.

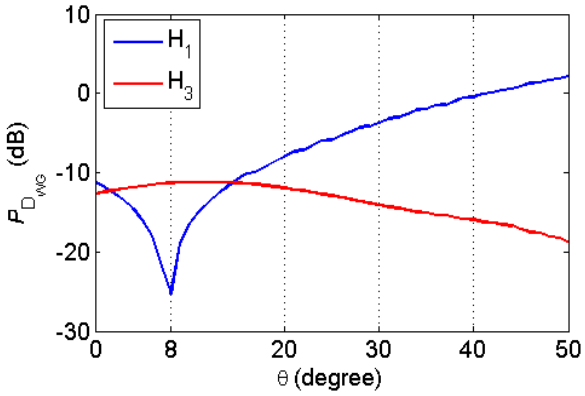

Fig. 8. Fundamental and third harmonic guided signals versus the angle of incidence for the configuration of Fig. 1.

Figure 7 shows plots of the magnitude of the x-component of the Poynting vector at $\lambda = 267nm$ at different cut through the structure as indicated by the red dashed lines. The Poynting flow was computed using $S_x = \frac{1}{2}\mathrm{Re}\left\{E(3\omega_0)\times H^*(3\omega_0)\cdot\hat{x}\right\}$. It clearly shows that the guided THS is mostly transformed into the TM_y mode of the waveguide. Figure 8 shows the guided power versus the angle of incidence for the input optical pulse. The optical pulse introduced here has a large broadening angle of $\Delta\theta = 8^\circ$ such that different resonances of Fig. 4 are not resolvable. The guided power for the fundamental harmonic exhibits a deep minimum at $\theta = 8^\circ$, which corresponds to the phase matching condition for larger conversion efficiency. However, the guided power of the THS shows a smooth and broadened resonance at the same angle. That is mainly due to the difference between the linear permittivity of the gold nanoparticles at the fundamental and third harmonics; i.e., $\varepsilon_r(\omega_0) = -26.2748 + 1.8493i$ and $\varepsilon_r(3\omega_0) = 0.44 + 9.75i$. The quality factor of any resonator made of such a medium at $\lambda = 800nm$ is larger than that of a resonator at $\lambda = 267nm$.

#156396 - $15.00 USD Received 12 Oct 2011; revised 9 Dec 2011; accepted 9 Dec 2011; published 9 Jan 2012

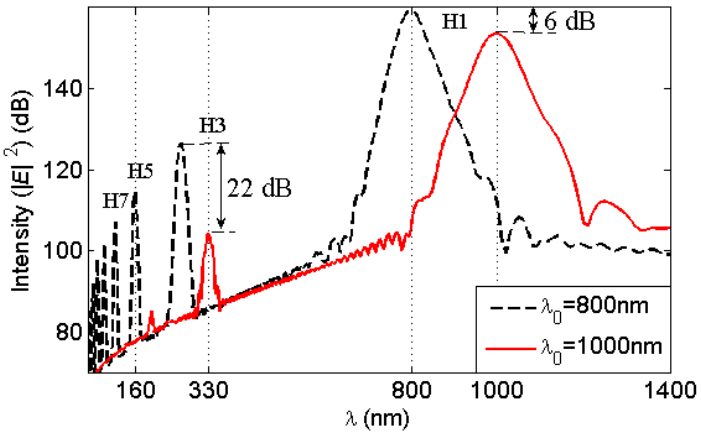

Fig. 9. Comparison between the intensity of the generated higher harmonics for on- and off-resonant excitations. The intensity has been computed at a distance of 10nm above the grating. For both cases, the structure has been excited with an s-polarized Gaussian optical pulse with the broadening of 1200nm and temporal duration of 50 fs, at the s-polarization.

Equation (2) shows that the local field enhancement factor due to the localized plasmonic resonances has a great impact on the conversion efficiency of third harmonic generation. This fact is investigated here by computing the average-intensity spectrum for illuminating the same structure with an optical pulse with a center wavelength of $\lambda_c = 1000nm$. The result is shown in Fig. 9. It is evident that the local field enhancement has affected the intensity of the generated harmonics. Although the difference in the intensity of the electric field at the fundamental frequency is only 6dB, the intensity of the THS decreases by 22dB, in comparison with the resonant excitation of $\lambda_c = 800nm$.

Another important factor to be considered is the propagation pattern of the generated third-harmonic beam inside the waveguide. Especially it is important to calculate the divergence angle of the third harmonic beam coupled to the waveguide. In order to do that, a finite array of 18 × 8 nano-rod antennas has been assumed. The other parameters, such as the dimensions of the nano-rod antennas, the height of the waveguide and the optical excitation are as before. Figure 10(a) and (b) show the field profile for the z-component of the electric field at a distance of 10 nm below the array and inside the waveguide, at the third-harmonic and fundamental frequencies, respectively.

#156396 - $15.00 USD Received 12 Oct 2011; revised 9 Dec 2011; accepted 9 Dec 2011; published 9 Jan 2012

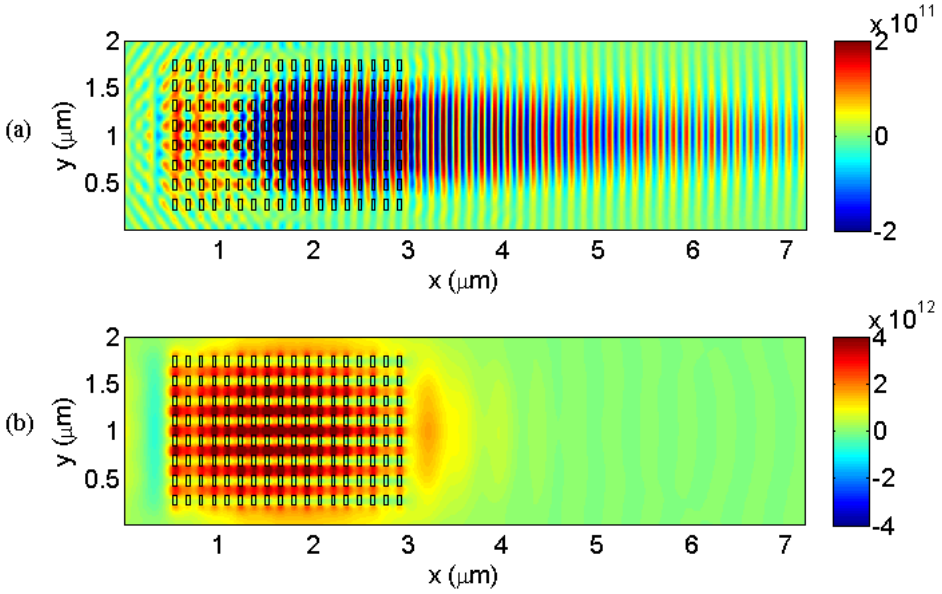

Fig. 10. Field profile for the z -component of the electric field at (a) third harmonic and (b) fundamental frequencies. The field profile is computed at a distance of 10nm below the array and inside the waveguide. The color bars are in arbitrary linear units. The structure is excited with an s-polarized Gaussian optical pulse with the broadening of 1200nm and temporal duration of 50 fs, at the central wavelength of 800nm.

Evidently, the grating of metallic nano-rod antennas exhibits characteristics of a lens, focusing the propagated third-harmonic radiation at a distance of approximately 4μm inside the waveguide. Moreover, it emerges from this figure that the size of the grating array has an important effect on the performance of this converter-coupler. From a practical point of view, the overall dimension of the array of nano-rod antennas should not exceed the spot size of theincident beam by much. Considering the time-reversed phenomenon, the guided third-harmonic radiation, diffracted by the grating in the absence of any incident radiation, will be coupled out of the waveguide into photonic modes above and below the structure. It is the interference of the THS propagated in the waveguide and that generated by the incident radiation, which gives rise to the anomalous extinction efficiencies observed in Fig. 4. If the domain of the array illuminated by the excitation beam would be much smaller than the whole array, a considerable amount of the propagating third-harmonic power will leak out of the waveguide. Figure 11 shows the guided power spectrum inside the waveguide, computed at a distance of 4 μm from the end of the array. The transmitted power is also shown in this figure. Evidently, the THS power propagating inside the waveguide is drastically higher than that at the fundamental frequency. The power scattered from the edges of the array, can hardly couple into the propagating modes of the waveguide, and is mostly radiated into the surrounding media. Considering the power spectrum of Fig. 11, a higher suppression of the fundamental beam at the output detector has been achieved than in the case of Fig. 6(a). On the one hand this is due to the larger grating in the second configuration. On the other hand, diffraction of the fundamental beam does not give rise to propagating modes in the waveguide. By considering even larger gratings and longer waveguides, still better suppression of the fundamental beam is possible.

In comparison with previously reported results, Fig. 11 shows rather good conversion efficiency of the third-harmonic generation process for the proposed configuration is about −35dB. For the 5th and 7th harmonics it is −45dB and −50dB, respectively. These values are higher than the conversion efficiency of −86dB reported in Ref [6]. for the 7th-Harmonic

#156396 - $15.00 USD Received 12 Oct 2011; revised 9 Dec 2011; accepted 9 Dec 2011; published 9 Jan 2012

generation, though it should be also mentioned that the experiment carried out in Ref [6]. is with an excitation intensity of 10^{11} W cm^{-2}. Moreover, a hybrid photonic-plasmonic waveguide has been proposed in Ref [3]. in a phase-matched configuration, to enhance the second-harmonic generation process inside a periodically-poled $LiNbO_3$. Since the fundamental and produced second-harmonics are both propagating through a lossy silver waveguide, the efficiency very much depends on the length of the structure. Using a waveguide length of only 3μm and an incident intensity of 10^7 W cm^{-2}, the reported conversion efficiency for the second-harmonic generation is about −33dB.

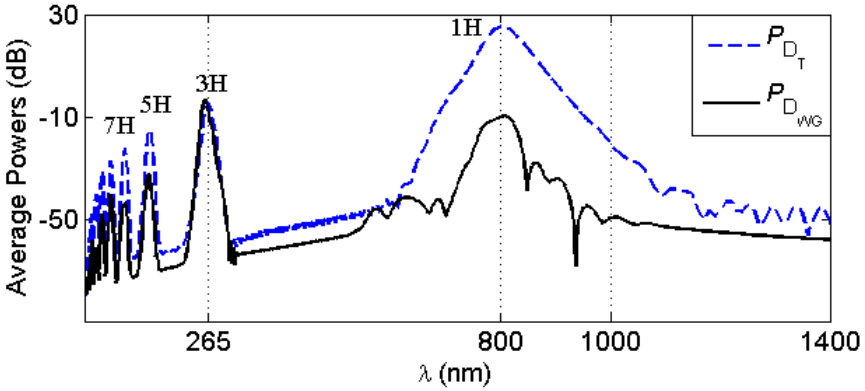

Fig. 11. The Power spectrum of the detected signals guided inside the waveguide and transmitted from structure. The grating is composed of 8x18 nano-rod antennas, as shown in Fig. 10. For the excitation, an optical Gaussian pulse with the broadening of 1200nm and temporal duration of 50 fs at the central wavelength of 1800nm has been used. The guided power is calculated at the location of 4μm from the end of the array.

4. Conclusion

We have proposed and analyzed the case of generating third harmonic radiation which is exclusively coupled into the propagating modes of a slab waveguide. By controlling the characteristics of grating anomalies, the phase-matching condition for coupling of the up-converted incident wave is achieved. At the same time, the fundamental frequency component is reflected off the grating.

Our study suggests an elegant separation of two crucial optical device design aspects through the use of metallic nano-particles: First, they individually generate harmonic frequency radiation of an incident wave. To this end, plasmonic particle resonances give a convenient boost to the up-conversion efficiency. Second, they can be arranged in a phase-matched array geometry to act as a coupler to further structures. Beyond simple waveguides, these can include resonators, mixers, de-multiplexers, etc.

Acknowledgments

N. Talebi and M. Shahabadi acknowledge the financial support of this project by Iran Telecommunication Research Center (ITRC).

#156396 - $15.00 USD Received 12 Oct 2011; revised 9 Dec 2011; accepted 9 Dec 2011; published 9 Jan 2012